International Journal of Biological Macromolecules 323 (2025) 147212

Contents lists available at ScienceDirect

International Journal of Biological Macromolecules

journal homepage: www.elsevier.com/locate/ijbiomac

Optimization, characterisation, and stability of chitosan-cellulose nanocrystal nanocomplexes

Rafaela Venâncio Flores [a,*], Meirielly Jesus [b], Joana Santos [b], Fernando Mata [b,c,**], Lucas de Souza Soares [d], Eduardo Basilio de Oliveira [a], Sukarno Olavo Ferreira [a], Taíla Veloso de Oliveira [a], Nilda de Fátima Ferreira Soares [a]

[a] Departamento de Tecnologia de Alimentos, Universidade Federal de Viçosa, Campus Universitário, s/n, CEP 36570-900 Viçosa, MG, Brazil
[b] CISAS - Centre for Research and Development in Agrifood Systems and Sustainability, Instituto Politécnico de Viana do Castelo, Rua da Escola Industrial e Comercial Nun'Alvares 34, 4900-347 Viana do Castelo, Portugal
[c] Estação Zootécnica Nacional, National Institute for Agricultural and Veterinary Research, I.P. (INIAV, I.P.), Fonte Boa, 2005-048 Vale de Santarém, Portugal
[d] Instituto de Ciências Agrárias, Universidade Federal de Viçosa, Campus Rio Paranaíba/, Rodovia MG 230, km 7, 38810-000 Rio Paranaíba, MG, Brazil

ARTICLE INFO

Keywords:
Functional food ingredients
Nanocarriers
Nanocrystalline cellulose
Polyelectrolyte complexes

ABSTRACT

The growing demand for sustainable and functional materials in the food industry has intensified the search for biodegradable systems capable of enhancing food quality, safety, and shelf life. In this context, this study aimed to develop and characterise polyelectrolyte complexes based on chitosan and nanocrystalline cellulose at varying molar ratios (3:1, 6.5:1, and 10:1), targeting their potential applications as delivery systems or functional ingredients in food formulations. The nano complexes were evaluated for physicochemical properties, colloidal behaviour, and thermal stability. Fourier transform infrared spectroscopy confirmed the formation of hydrogen bonding interactions between the biopolymers, while thermogravimetric analysis demonstrated the enhanced thermal stability of the polyelectrolyte complexes compared to the individual polymers. Long-term stability tests conducted over 30 days at 7 °C and 25 °C revealed that the 3:1 ratio produced the most stable dispersion, with minimal aggregation and consistent particle size. These results highlight the potential of CHI:CNC nanocomplexes, particularly at a 3:1 ratio, as promising, thermally stable, and biocompatible systems for applications in food technology aimed at improving the performance and shelf stability of bioactive compounds.

1. Introduction

The demand for products and ingredients with broad applications focused on performance and effectiveness in the food and pharmaceutical sectors has driven the development of innovative delivery systems, such as nanoparticle carriers, hydrogels, and nanocomplexes. These technologies aim to enhance the functionality, bioavailability, and stability of active compounds. In parallel, the growing need for sustainable production has intensified interest in the use of eco-friendly materials derived from natural and renewable sources. In this context, polyelectrolytes have emerged as a promising strategy, attracting attention as one of the most compelling sustainable research topics and technological innovations [1]. Polyelectrolytes are formed through electrostatic interactions between oppositely charged polymers, as well as surfactants and chemical ligands, offering a green and efficient pathway to fabricate functional materials [2,3].

Among natural polyelectrolytes (PECs), chitosan and cellulose nanocrystals (CNC) have demonstrated remarkable potential for the development of functional systems. Chitosan is a natural polymer that consists of glucosamine residues linked by β-1,4 bonds and randomly distributed *N*-acetyl-D-glucosamine units. It is the second most abundant polymer in the world, valued for its non-toxicity, biocompatibility, biodegradability, and film-forming properties [3,4]. The cationic nature of chitosan enables it to form complexes with a range of anionic polymers and other chemical compounds through ionic gelation, such as sodium alginate [5], carboxymethylcellulose [6], cellulose nanocrystals [7], glutaraldehyde, and sodium tripolyphosphate [8], while pure chitosan nanoparticles can be produced through desolation process, which

* Corresponding author.
** Correspondence to: F. Mata, CISAS - Centre for Research and Development in Agrifood Systems and Sustainability, Instituto Politécnico de Viana do Castelo, Rua da Escola Industrial e Comercial Nun'Alvares 34, 4900-347 Viana do Castelo, Portugal.
E-mail addresses: rafaela.flores@ufv.br (R.V. Flores), fernandomata@ipvc.pt (F. Mata).

https://doi.org/10.1016/j.ijbiomac.2025.147212
Received 12 June 2025; Received in revised form 26 August 2025; Accepted 27 August 2025
Available online 28 August 2025

is bases on precipitation. CNC, in turn, is derived from the acid hydrolysis of cellulose fibres, yielding rod-like particles with high crystallinity, aspect ratio (length/diameter), and surface area [9]. To produce CNC, sulphuric acid is commonly used in the hydrolysis of cellulose fibres, allowing the amorphous regions of the polymer chain to be removed the amorphous phase and to be functionalized with sulphonate groups or to expose free hydroxyl groups, providing CNC with an anionic character that is pH-dependent [10].

Regarding chitosan-based nanocomplexes and other natural polymers, many authors report low mechanical strength [11], the formation of porous hydrogels [12], and metastable systems [7,13]. It is known that several factors influence the formation of chitosan-based nanocomplexes, such as pH, ionic strength, molecular weight of chitosan, polymer ratio, and stirring speed [11], however the combined effect of these factors remains underexplored, impacting methodological replication, reproducibility, stability, and encapsulation efficiency of the systems [14,15]. In this context, aiming to evaluate simultaneously the influence of multiple variables, the present study aimed, for the first time, to optimise the production process of chitosan–CNC nanocomplexes (CHI:CNC) using a Box–Behnken design, focusing on three critical parameters such as the monovalent salt concentration, the molar ratio of ionisable groups, and the pH on the physicochemical, thermal and structural properties. A key differentiator of this study lies in the comprehension of the pure chitosan–nanocrystalline cellulose nanocomplex system, independent of any specific active compound, providing essential fundamental insights about the impact of the factors on the complexation, stability and reproducibility of the system. Therefore, this study can support the application of chitosan-nanocellulose complexes as functional ingredients or delivery systems to improve food quality, safety, and shelf life. Furthermore, the complexes enable the production of materials with high adsorption capacity, tunable mechanical properties, biodegradability, and biocompatibility for application as active packaging, in regenerative medicine for drug delivery and water treatment, which should be investigated through future works.

2. Materials and methods

2.1. Material

Chitosan (low molecular weight ~50–190 kDa, ~75–85 % Deacetylation Degree - DD, ≈0 % Sulfonation Degree - SD, Sigma-Aldrich Corporation, USA; Product ID: 448869), derived from fresh shrimp shells *Pandalus borealis*, was purchased from Sigma-Aldrich Corporation (USA). Cellulose nanocrystals (CelluForce, Canada; Product ID: NCV100, 2–5 nm diameter, 100 μm length, 200–8000 kDa) were obtained from CelluForce Corporation (Canada). All other chemicals were of analytical grade and used without further purification: hydrochloric acid (Neon, Brazil, 37 wt% in H_2O), sodium chloride (FMaia, Brazil, 99 % purity), and sodium hydroxide (Dinâmica, Brazil). Milli-Q water (18.2 MΩ·cm at 25 °C) was produced using a Milli-Q system (Millipore, Italy) and used in all experiments.

2.2. Experimental design

A Box–Behnken experimental design was employed to investigate the effects of the molar ratio between chitosan and cellulose nanocrystals (CHI:CNC), the pH of CNC (pH), and the molar concentration of NaCl ([NaCl]), as well as the interactions among these independent variables, on particle size (nm), zeta potential (mV), and yield (%). The level of the factors was selected to achieve a wide area, maintaining the pH at acidic conditions, favouring the chitosan solubility. The CHI:CNC ratios of 3:1, 6.5:1, and 10:1 were selected based on the stoichiometric balance of ionizable groups (amino and sulfonate groups) in each polymer, considering the theoretical charge density of both chitosan and sulfonated CNC. A design matrix consisting of 13 experimental runs was constructed, with the resulting systems from the combination of the independent variables summarised in Table 1. The central point (CP) was represented by the 13th system, and five replicates were performed at this point.

2.3. Preliminary chitosan characterisation

2.3.1. Chitosan purification

Initially, chitosan was subjected to a purification process aimed at reducing water-soluble chitooligosaccharides and salt residues present in the product batch. The chitosan was washed three times with Milli-Q water and recovered using a vacuum filtration system with qualitative filter paper (Cat. No. 1004 125, Whatman) [6,16]. Subsequently, the chitosan was frozen at −80 °C, lyophilised (FreeZone, 2.5 L, LABCONCO), vacuum-packed, and stored in a desiccator at 20 °C.

2.3.2. Determination of the viscosity-average molar mass

The viscosity-average molar mass (Mv) of chitosan was estimated using the capillary viscometry technique [16,17]. For this, 0.25 g of chitosan was dispersed in 100 mL of acetate buffer (0.2 M acetic acid + 0.1 M sodium acetate; pH = 4.41; ionic strength = 0.1 M) [18] and stirred magnetically for 24 h. The resulting chitosan dispersion was then vacuum filtered (vacuum pump MA039; Marconi®, Brazil) using a Buchner funnel fitted with qualitative filter paper. Based on this dispersion, four dilutions were prepared (0.05, 0.10, 0.15, and 0.20 g·100 mL^{-1}). A Cannon-Fenske capillary *v*iscometer (model 513 10, Schott®, Germany) was used to measure the flow time of 10 mL of each dilution at 25.0 ± 0.1 °C. The intrinsic viscosity ($\overline{[\eta]}$) was then calculated, and from the experimental data, the viscosity-average molar mass was estimated to be 463 ± 25 kDa (for details, see Supplementary Material; Figure SM1).

2.3.3. Determination of the degree of deacetylation and amino group density (NH_3^+)

Chitosan powder was analysed using Fourier transform infrared (FTIR) spectroscopy. The degree of acetylation (DA) was then estimated from the empirical relationship between the normalized absorbances of the peaks at wavenumbers 1320 and 1420 cm^{-1}, following deconvolution into Lorentzian components using PeakFit software (v.4.12, SeaSolve Software Inc., 1999–2003) [18,19]. The degree of deacetylation (DD) was calculated by simple subtraction [DD(%) = 100 % – DA(%)], and the DD of the chitosan used in this study was estimated to be 69.10 %.

Subsequently, the amino group content of the chitosan was determined using Eq. (1), yielding a *v*alue of 3.9681 ± 0.54 mol·kg^{-1}.

Table 1
Coded and uncoded variables of Box-Behnken experimental design used to optimise the formation of the chitosan-nanocrystalline cellulose nanocomplexes.

Systems	Coded variables			Uncoded variables		
	CHI:CNC (mol) (X_1)	pH (X_2)	[NaCl] (mM) (X_3)	CHI:CNC (mol) (X_1)	pH (X_2)	[NaCl] (mM) (X_3)
1	−1	−1	0	3	2.6	37.5
2	1	−1	0	10	2.6	37.5
3	−1	1	0	3	5	37.5
4	1	1	0	10	5	37.5
5	−1	0	−1	3	3.8	0
6	1	0	−1	10	3.8	0
7	−1	0	1	3	3.8	75
8	1	0	1	10	3.8	75
9	0	−1	−1	6.5	2.6	0
10	0	1	−1	6.5	5	0
11	0	-1	1	6.5	2.6	75
12	0	1	1	6.5	5	75
13[a]	0	0	0	6.5	3.8	37.5

[a] Central point (CP) of Box-Behnken experimental design. CHI:CNC – chitosan to nanocrystalline cellulose ratio.

$$\frac{n_{NH_3^+}}{m_{CHI}} = \frac{DD}{DD \times MM_D + (1 - GD) \times MM_A} \quad (1)$$

In which $n^+_{NH_3}$ is the number of moles of amino groups in the chitosan; $m_{(CHI)}$ is the mass of the chitosan; DD is the degree of deacetylation of the chitosan; $M_{(D)} = 161.1558\ g{\cdot}mol^{-1}$ is the molar mass of the deacetylated unit of chitosan; and $M_{(A)} = 203.1925\ g{\cdot}mol^{-1}$ is the molar mass of the acetylated unit of chitosan.

2.4. Preliminary characterisation of cellulose nanocrystals

2.4.1. Determination of sulphonate group density (-O-SO₃⁻)

The determination was carried out according to the method described by [20], in which a 0.55 % *w/v* suspension of CNC was prepared and dialysed using Milli-Q water for 3 days, with successive water changes until both pH and conductivity were constant and comparable to those of Milli-Q water.

DOWEXTM MonosphereTM 88 H cation exchange resin (DOW Chemical Company, USA) was used following the dialysis process to ensure full protonation of the sulphate semi-ester groups on the surface of the CNC. This treatment replaced all residual cations and anions with protons and hydroxide ions, respectively, thereby enabling an accurate estimation of the surface charge [20].

The recovered dispersion was then diluted to yield 0.15 g of solids. One-third of the diluted dispersion was transferred into a 100 mL volumetric flask, along with 2 mL of 0.1 M NaCl solution, and the volume was completed with Milli-Q water. The sulphonate group density of the CNC was determined via conductometric titration using a conductivity meter (145A+, Thermo, Orion, USA). Samples were titrated with standardised 0.1 M NaOH (standardised using potassium hydrogen phthalate), and the equivalence point was identified graphically (see graph provided in the Supplementary Material).

All measurements were performed in triplicate. The sulphonate group density of the cellulose nanocrystals used in this study was determined to be 216.87 ± 9.01 mmol $(OSO_3^-){\cdot}kg^{-1}$ (for details, see Supplementary Material; Fig. SM3).

2.5. Preparation of biopolymer dispersions and formation of nanocomplexes

Previously, 0.5 $mg{\cdot}mL^{-1}$ CHI was mixed with a 0.6343 $mol{\cdot}L^{-1}$ HCl solution (pH = 3.0), and this material was kept under magnetic stirring at 25 °C for 24 h. Then, the CHI dispersion was filtered using a black ribbon quantitative filter, followed by a second filtration using a blue-ribbon quantitative filter. Amounts of NaCl (Table 1) were added to the CH dispersions, and the resulting aqueous media were stirred for an additional 2 h. Finally, the CH dispersions containing NaCl were filtered according to the aforementioned procedure.

Analogously, 1.0 $mg{\cdot}mL^{-1}$ CNC was added to deionised water, placed into an ice bath, and dispersed using an ultrasound device (Unique, disruptor model – 19 kHz, 420 W) for 10 min. Then, the CNC dispersion was filtered using a 0.45 μm syringe filter (Millipore), and appropriate amounts of NaCl (Table 1) were added to the aqueous media. The pH of CH or CNC dispersions was adjusted to values from 2.6 to 5.0 (Table 1), using 1 $mol{\cdot}L^{-1}$ NaOH or 1 $mol{\cdot}L^{-1}$ HCl.

During the preparation of the nanocomplexes, appropriate amounts of CNC dispersions were added to 5 mL of CH dispersions (Table 1) at a rate of 0.5 $mL{\cdot}min^{-1}$, using a 0.13 mm × 45 mm syringe coupled with a peristaltic pump (TECNOPON, LAP-101-3 model). The CHI dispersion was kept under magnetic stirring during CNC addition, and the agitation was maintained for 10 min after the completion of CNC addition. Systems containing CH and CNC were placed in 50 mL Falcon tubes and centrifuged at 13,000 ×*g* at 4 °C for 30 min. Then, the supernatants were removed, and the pellets were added to deionised water, placed into an ice bath, and redispersed using an ultrasound device (420 W) for 6 min. The resulting systems were stored at 7 °C prior to further use.

2.6. Yield (%) of nanocomplexes

Firstly, the weight of empty 50 mL Falcon tubes was recorded. Then, aliquots of the systems were transferred to these tubes, and their weight was recorded again. After centrifugation at 13,000 ×*g* at 4 °C for 30 min, the supernatants were removed, and the nanocomplexes remaining at the bottom of the tubes were weighed together with the tubes. The yield (Y, %) was then calculated using Eq. (2).

$$Y(\%) = \frac{W - W_0}{W_D - W_0} \times 100 \quad (2)$$

In which W_o is the weight of 50 mL Falcon tubes empty, W_D is the weight of 50 mL Falcon tubes containing the systems, and W is the weight of 50 mL Falcon tubes containing the nanocomplex.

2.7. Particle size, polydispersity index, and ζ potential

The particle size, PDI, and ζ potential of CHI, CNC, and nanocomplex dispersions were evaluated by dynamic light scattering (DLS) using a Zetasizer Nano ZS90 (Malvern Instruments, UK) at 25.0 ± 0.1 °C. Aliquots of the aqueous media were placed in a cuvette to obtain the particle size distribution based on the amplitude of the decay rate, which is determined by fitting the normalized temporal intensity correlation functions. This analysis was performed in triplicate. The polydispersity index (PDI) was then calculated. PDI was estimated from the relationship between the hydrodynamic average diameter (d_h) and the standard deviation (SD) using the formula $PDI = (SD/d\_h)^2$ for each particle distribution.

The ζ potential of the dispersed particles was estimated from their electrophoretic mobility. Aliquots of the aqueous media were placed into a folded capillary cell (DTS1070; Malvern Instruments, UK) and analysed using the Zetasizer Nano ZS90. The cuvette was subjected to a controlled electric field, and ζ potential values were calculated using the Smoluchowski model for the electrical double layer.

2.8. Atomic force microscopy

To study the size and morphology of the nanoparticles, a drop of the appropriately diluted nanoparticle suspension was spread onto a mica surface and dried at room temperature. After solvent evaporation, the samples were analysed using an atomic force microscope (NT-MDT, INTEGRA PRIMA, Russia). Measurements were carried out in intermittent contact mode, using a probe with a tip curvature radius of 10 nm, a force constant of 10 N/m, and a resonance frequency of approximately 280 kHz 16.

2.9. X-ray diffractometry

The X-ray Diffractometry (XRD) patterns of CHI, CNC, and nanocomplexes (CHI:CNC = 3:1, 6.5:1, or 10:1) were examined using an X-ray diffractometer (D8 Advance, Bruker, Germany) equipped with Cu-Kα radiation (λ = 0.1542 nm), operating at 40 kV and 40 mA. Scans were recorded over a 2θ range of 10° to 50°, at a scanning rate of 0.5 $degrees{\cdot}s^{-1}$. The obtained diffractograms were analysed, and differences between them indicated the formation of nanocomplexes. Furthermore, XRD analysis was employed to evaluate the influence of the CHI:CNC ratio on the degree of crystallinity and the presence of amorphous regions in the nanocomplexes. The crystallinity index (CI, %) was then calculated as proposed by Segal et al. [21] (Eq. (3)):

$$CI(\%) = \frac{I_{002} - I_{am}}{I_{002}} \times 100 \quad (3)$$

where I_{002} is the maximum intensity (arb. u.) of the 002-lattice diffraction, and I_{am} is the intensity of diffraction in the same units at 2θ = 18°.

2.10. Attenuated total reflectance Fourier-transform infrared spectroscopy

Fourier-Transform Infrared Spectroscopy analyses were performed using a spectrophotometer (Nicolet 6700, Thermo Scientific, USA) to study the molecular interactions between CH and CNC in the nanocomplexes. Spectra were recorded in the range of 4000 cm^{-1} to 400 cm^{-1}, with a spectral resolution of 4 cm^{-1} and 32 accumulated scans per spectrum. Thus, pellets obtained after centrifugation were previously freeze-dried, and the analyses were carried out directly on the nanocomplexes.

2.11. Thermogravimetric analysis

The thermal behaviour of CHI, CNC, and nanocomplexes (CHI:CNC = 3:1, 6.5:1, or 10:1) was evaluated using a thermogravimetric analyser (Shimadzu, 60H, Japan). Freeze-dried samples (3–5 mg) were weighed using the thermogravimetric analysis (TGA) microbalance and heated from 25 °C to 700 °C at a rate of 20 °C·min^{-1}. Nitrogen gas was used as the purge medium, with a flow rate of 20 mL·min^{-1}.

2.12. Macroscopic and microscopic stability

The stability of the systems (CHI:CNC = 3:1, 6.5:1, or 10:1) stored at 7 °C or 25 °C was monitored over 30 days [22]. Initially, changes in the visual appearance of the systems and Tyndall scattering effects were observed. Subsequently, the zeta potential, Particle size, and PDI of the nanocomplexes were also assessed.

2.13. Data analysis

Statistical analyses were performed using Minitab software, version 17.0 (Minitab Software Systems, State College, PA). Response Surface Methodology (RSM) was applied to the experimental data to optimise nanocomplex formation and assess the effects and/or interactions of the independent variables (CHI:CNC ratio, pH, and [NaCl]) on the dependent responses (Particle size, zeta potential, and yield). A nonlinear quadratic model was fitted as shown in Eq. (4):

$$Y = b_0 + b_1X_1 + b_2X_2 + b_3X_3 + b_{12}X_1X_2 + b_{13}X_1X_3 + b_{23}X_2X_3 + b_{11}{X_1}^2 + b_{22}{X_2}^2 + b_{33}{X_3}^2 \quad (4)$$

In which Y is the measured response associated with each factor-level combination; b_0 is the intercept; b_1 to b_{33} are regression coefficients determined from the observed experimental values; X_1 is the molar ratio between chitosan and CNC (CHI:CNC), X_2 is the pH, and X_3 is the NaCl molar concentration ([NaCl]). The terms X_1X_2, X_1X_3, and X_2X_3 represent interaction effects, while ${X_1}^2$, ${X_2}^2$, and ${X_3}^2$ are the quadratic terms.

Regression models were also used to investigate the interaction between storage temperature and time on the dependent variables: zeta potential, Particle size, and PDI.

Macroscopic visual aspects and Tyndall effects were described qualitatively. Data obtained from AFM, XRD, ATR-FTIR, and TGA analyses of the nanocomplexes were compared with those of CHI and CNC, and the results were presented in qualitative terms.

3. Results and discussion

3.1. Optimisation

To optimise nanocomplex formation by reducing particle size and increasing zeta potential and yield, a Box–Behnken experimental design was applied, involving the independent variables CHI:CNC ratio, pH, and [NaCl]. The results for Particle size, PDI, zeta potential, and yield obtained from the experimental design are presented in Table 2.

According to Table 2, all systems exhibited suitable values for particle size (151–195 nm), zeta potential (+44.6 to +51.3 mV), and PDI (≤0,3), being considered ideal for applications in both the food and pharmaceutical sectors [23].

Smaller particle diameters enhance adhesion and penetration through cell membranes, allowing for more controlled release of bioactive and therapeutic compounds encapsulated within these structures [23], thereby improving their efficiency. Regarding zeta potential, all nanocomplexes formed (Table 2) exhibited positive values, indicating the predominance of chitosan structures on the surface of the nanocomplexes. In the context of zeta potential analysis, nanoparticles and nanocomplexes with surface charge values above ±30 mV are considered more stable, as this charge is sufficient to prevent particle aggregation [44]. Finally, concerning PDI, values below 0.3 indicate high homogeneity in the particle size distribution.

To investigate the effects of the independent variables (CHI:CNC ratio, pH, and [NaCl]) on the dependent responses (particle size, zeta potential, and yield), regression model coefficients were estimated and are shown in Table 3. Additionally, contour plots are presented in Fig. 1.

The responses were individually fitted using linear regression to obtain the models with the best fit and highest coefficient of determination (R^2). ANOVA was conducted to identify the statistically significant terms in each model. Model terms with $p < 0.05$ were considered statistically significant. However, given the high R^2 values of the models and to preserve the realism of the results, non-significant terms were retained in the models (Eqs. (5), (6) and (7)).

$$\text{Particle size} = 127.983 + 0.898\,X_1 + 0.032\,X_2 + 2.237\,X_3 - 0.102\,X_1X_2 - 0.488\,X_1X_3 - 0.053\,X_2X_3 + 0.365\,{X_1}^2 + 0.011\,{X_2}^2 + 1.915\,{X_3}^2 \quad (5)$$

$$\text{Zeta} - \text{potential} = 37.137 + 0.569\,X_1 + 0.065\,X_2 + 4.121\,X_3 + 0.015\,X_1X_2 + 0.014\,X_1X_3 - 0.017\,X_2X_3 - 0.071\,{X_1}^2 - 0.001\,{X_2}^2 - 0.482\,{X_3}^2 \quad (6)$$

$$\text{Yield} = -2.166 + 0.123\,X_1 + 0.166\,X_2 + 2.115\,X_3 - 0.003\,X_1X_2 - 0.010\,X_1X_3 - 0.045\,X_2X_3 \quad (7)$$

In which, X_1 = CHI:CNC, X_2 = pH, and X_3 = [NaCl].

A quadratic model was fitted to the particle size and zeta potential data, while a two-factor interaction (2FI) model was applied to the yield data. All models were statistically significant ($p < 0.05$), exhibited R^2 values >0.7, and showed no significant lack of fit.

For particle size, the quadratic model revealed positive effects of CHI:CNC ratio, pH, and NaCl concentration, with a significant negative interaction between the factors ($p < 0.05$, Fig. 1C). All quadratic terms contributed positively to particle size, resulting in nanostructures smaller than 200 nm. The interaction between CHI:CNC and NaCl concentration resulted in the lowest particle size values observed under two

Table 2
Particle size, Zeta-potential and Yield values for systems of the Box-Behnken experimental design.

System	CHI:CNC	pH	[NaCl] (mM)	Particle size (nm)	PDI	Zeta-potential (mV)	Yield (%)
1	3	2.6	37.5	151.23	0.27	47.60	5.07
2	10	2.6	37.5	156.23	0.26	49.47	5.83
3	3	5	37.5	178.40	0.28	45.87	5.71
4	10	5	37.5	175.20	0.28	47.97	6.30
5	3	3.8	0	164.70	0.26	46.83	7.01
6	10	3.8	0	189.97	0.3	44.57	6.66
7	3	3.8	75	193.87	0.27	45.73	4.69
8	10	3,8	75	165.47	0.27	51.30	2.59
9	6.5	2.6	0	157.80	0.3	45.13	2.80
10	6.5	5	0	195.33	0.29	47.90	8.05
11	6.5	2.6	75	163.03	0.26	48.17	6.14
12	6.5	5	75	191.00	0.26	47.93	3.33
13*	6.5	3.8	37.5	158.04	0.27	49.29	5.87

Note: PDI - polydispersity index; CHI:CNC – Chitosan: nanocrystalline cellulose ratio.

conditions (Fig. 1D): (i) higher NaCl concentrations combined with higher CH:CNC ratios, and (ii) lower NaCl concentrations combined with lower CHI:CNC ratios. This suggests that, to achieve particle diameters as low as 160 nm, a balance between the maximum usable NaCl concentration and the CNC dispersion must be considered. One possible explanation is that the ionisation degree of CNC and chitosan differs at the same pH. For example, at pH 3.8, chitosan is more ionised and adopts a more extended conformation compared to CNC. Consequently, the presence of an electrolyte may partially neutralise excess charges, allowing chitosan molecules to adopt a less stretched conformation, which results in partial folding of the formed particles [24].

Regarding zeta potential, the factors also had significant positive effects, including significant interactions between CHI:CNC and pH (Fig. 1B), and between CHI:CNC and NaCl (Fig. 1A), which provided an increase in zeta potential values under conditions of higher CHI:CNC ratios and higher NaCl concentrations. This confirms the minor influence of NaCl addition on the surface charge density of the nanocomplexes. A similar finding was reported by Prathapan et al. [25], who observed that Na^+ and Cl^- ions did not significantly affect the zeta potential of cellulose nanocrystals when the dispersion pH was either strongly acidic or basic. Instead, more hydrophobic ions from the Hofmeister series had a greater impact in reducing the zeta potential of such colloidal particles.

In contrast, the interaction between pH and NaCl concentration had a negative effect, as expected for polyelectrolytes such as chitosan and CNC. Changes in the pH alter the degree of ionisation in both chitosan and CNC, thereby intensifying Coulombic interactions. However, a simultaneous increase in the ionic strength of the medium can reverse this behaviour, as ion concentration can attenuate the charges of polyelectrolytes [24]. Despite these findings, it is evident that, regardless of

Table 3
Descriptive statistics, regression models for Particle size, Zeta-potential or Yield (%), and fitting indicators of models.

Variable	Mean	SD	Model	F-value	*p*-Value	R^2	Lack of fit
Particle size	168.97	4.53	Quadratic	19.4	0.0004	0.9615	0.5768[a]
Zeta-potential	47.94	0.98	Quadratic	5.52	0.0174	0.8765	0.1047[a]
Yield (%)	5.45	1.00	2FI	4.35	0.0300	0.7655	0.4117[a]

[a] Not significant; SD – standard deviation.

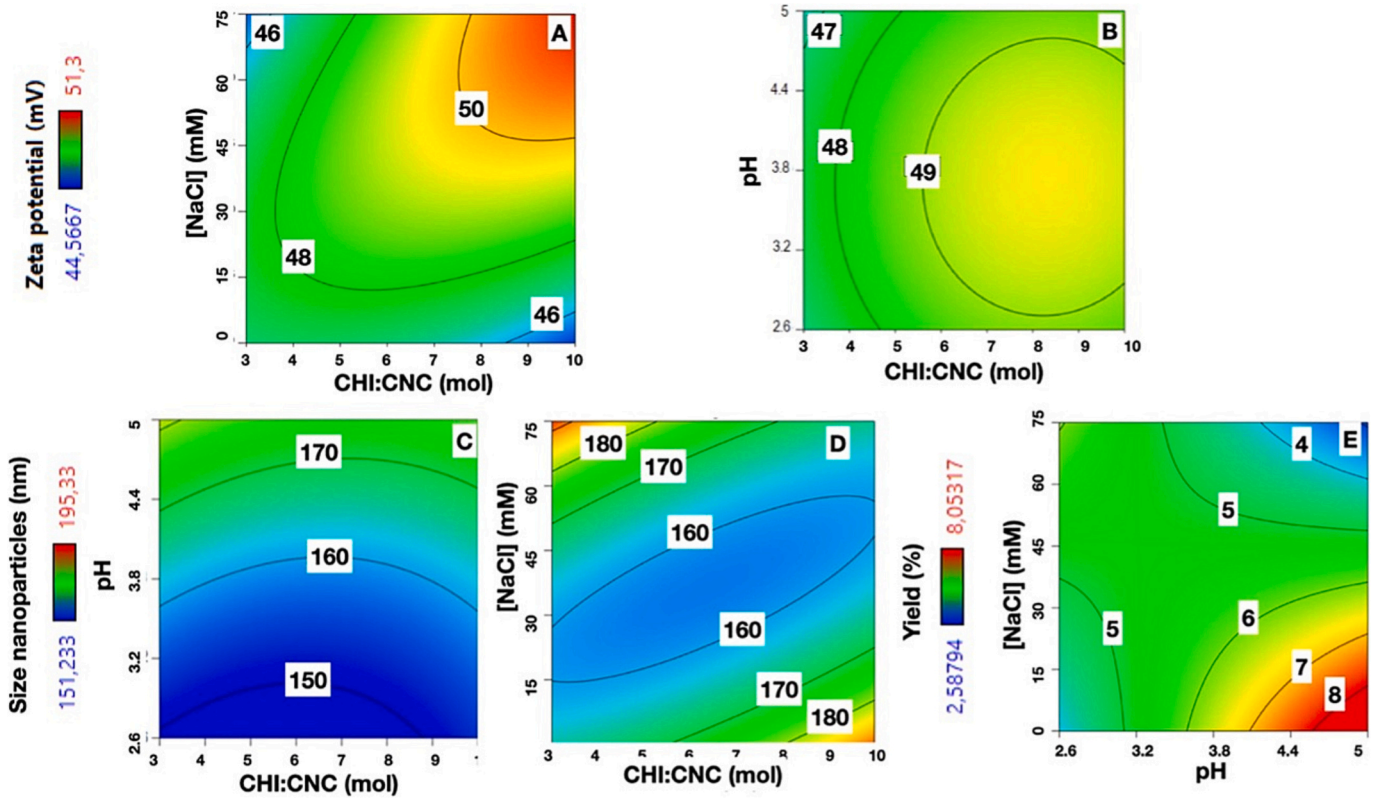

Fig. 1. Contour graphics for Zeta-potential (A and B), Particle size (C and D), and Yield (E). Chitosan: nanocrystalline cellulose ratio (CH:CNC).

the levels of the studied variables, the zeta potential remained positive and above +40 mV, which suggests high stability of the nanocomplexes in dispersion. Therefore, to optimise this response variable under the studied conditions, lower CHI:CNC ratios could also be used to produce nanocomplexes in the absence of NaCl.

For yield, the model indicated positive main effects of CHI:CNC ratio, pH, and NaCl concentration, while thee interactions CHI:CNC*pH, CHI:CNC*[NaCl], and pH*[NaCl] showed negative effects. Fig. 1E shows that higher yields were obtained at higher pH values and lower NaCl concentrations. For example, NaCl concentrations up to ~10 mM and CNC dispersion pH between 4.5 and 5.0 resulted in nanocomplex yields of approximately 8 %. Given that nanocomplexes are developed for use in food, pharmaceutical, and cosmetic industries, high yield is a key factor for process scale-up. Therefore, the best formulations were selected based on this response variable.

Furthermore, based on the characterisation and stability results, the smallest particle size and the highest zeta potential were obtained at pH 5.0, in the absence of NaCl, independent of the CHI:CNC ratio. Therefore, the study continued using all the three ratios 3:1, 6.5:1, and 10:1 for subsequent thermal stability evaluations. This approach allowed us to focus on differentiating the nanocomplexes according to other critical properties—such as crystallinity, intermolecular interactions, thermal properties, and stability behaviour—providing deeper insights into how formulation parameters influence system robustness and guiding their potential application in food and pharmaceutical systems.

3.2. Atomic force microscopy

The morphology of the nanocomplexes was analysed using atomic force microscopy (AFM). Sample preparation for this analysis requires drying the suspensions on glass slides. Due to the surface tension of water on glass, the suspended particles tend to migrate towards the edges of the water droplet, where they aggregate and form distorted images. This can hinder accurate identification of the materials under investigation.

In Fig. 2A, the needle-like structure of an isolated cellulose nanocrystal is visible, with an approximate height of 2 nm, confirming the nanodimension and elongated shape of the nanocomplexes. Micrographs 2B, 2C, and 2D correspond to nanocomplexes at a molar ratio of CHI:CNC 10:1, and display an oval morphology, with dimensions ranging between 20 and 30 nm.

When comparing the average diameters observed for both the CNC and the nanocomplexes with those obtained by DLS, a considerable difference between the values is evident. The larger average diameter

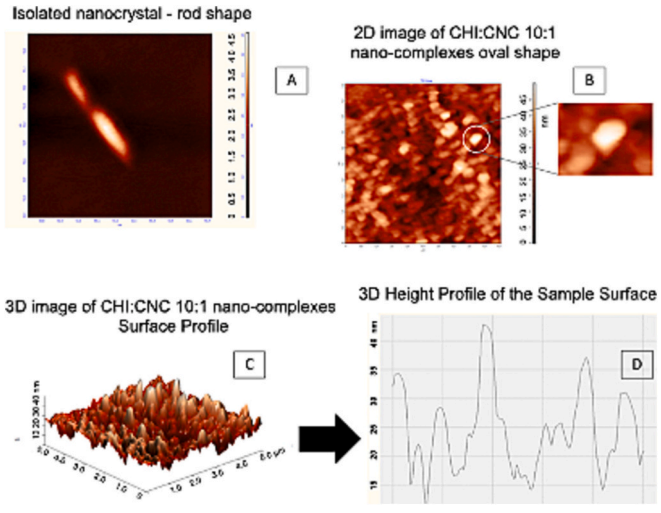

Fig. 2. Atomic force microscopy images of chitosan; nanocrystalline cellulose nanocomplex at 10:1 ratio.

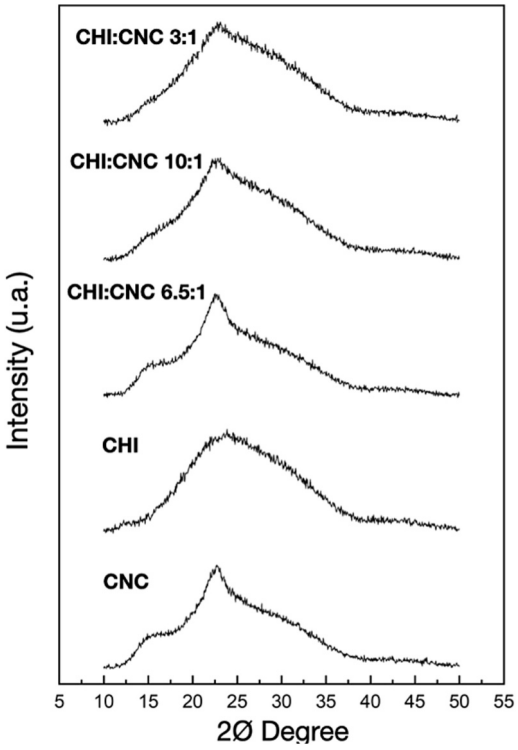

Fig. 3. X-ray diffractograms of chitosan (CH), nanocrystalline cellulose (CNC), and CH:CNC nanocomplexes at different molar ratio.

estimated by DLS can be attributed to the measurement principle, which is based on the movement and drag of particles in dispersion, taking into account the electrical double layer. This contributes to an increase in the calculated particle diameter.

A similar discrepancy was reported by Mukhopadhyay et al. [26] when studying the incorporation of insulin into chitosan nanoparticles crosslinked with tripolyphosphate. In their study, particle sizes ranged between 80 and 120 nm as measured by AFM, but between 200 and 550 nm by DLS. This discrepancy was attributed to the fact that the hydrodynamic diameter of freshly prepared nanoparticles measured by DLS is larger than the microscopic estimate due to the swelling effects of the produced nanoparticles.

3.3. X-ray diffractometry

Fig. 3 illustrates the diffractograms of the nanocomplexes and their individual components. The corresponding crystallinity indices were calculated from the presented diffractograms.

Chitosan exhibited two characteristic peaks at $2\theta = 19.85^\circ$ and $2\theta = 21.75^\circ$, corresponding to the (020) and (120) planes, respectively, which is consistent with results reported by other researchers [6,27,28]. The crystallinity degree of chitosan was 47.89 %, indicative of a semi-crystalline material resulting from strong inter- and intramolecular interactions, mainly hydrogen bonding, established between amino, hydroxyl, and amide groups. These interactions contribute to a higher degree of organisation in the chitosan molecular structure [29]. Additionally, it is known that chitosan properties such as molecular weight, degree of deacetylation, and density of amino groups strongly influence its physicochemical and structural characteristics [30].

Regarding the nanocrystals, these were characterised primarily due to their well-known cellulose I crystalline structure, with peaks at 2θ values centred at 15.05°, 16.35°, and 22.5°, attributed to the (−110), (110), and (200) planes [31]. Another peak of lower intensity at $2\theta = 34.5^\circ$ was also identified (Fig. 3). This peak can be attributed to diffraction from the (004) plane [32]. The crystallinity index of the CNC

was 79.33 %, close to the value specified by the manufacturer (Ic = 88 %).

As for the nanocomplexes, these exhibited broader, more diffuse peaks with less pronounced signals at 2θ = 15° and 2θ = 16°, and the disappearance of peaks at 2θ = 34.5° (attributed to CNC) and 2θ = 21.75° (attributed to chitosan). This indicates rearrangement of the polymer chains during nanocomplex formation, resulting in changes to the crystalline structure. The XRD results corroborate the AFM findings, which also show the formation of new structures. Further evidence of nanocomplex formation is the reduction in the intensity of the peak at 19.8° as the molar amount of NH_3^+ groups from chitosan decreases relative to CNC, with this reduction being more pronounced at a molar ratio of CHI:CNC = 3:1. This can be explained by the closer matching of interaction sites between chitosan and CNC, causing a significant portion of chitosan in the medium to engage with CNC, thereby altering the arrangement of crystals within the nanocomplexes.

This observation is further supported by the crystallinity values of the nanocomplexes, which were 68.6 %, 51.84 %, and 37.3 % for NP 10:1, NP 6.5:1, and NP 3:1, respectively. The increase in crystallinity of the nanocomplexes also implies a greater organisation of the supramolecular structure formed.

3.4. Infrared spectroscopy

The chemical structure of the nanocomplexes was analysed by infrared spectroscopy, with their spectra shown in Fig. 4. The spectra of chitosan and cellulose nanocrystals were similar due to the resemblance in their molecular structures.

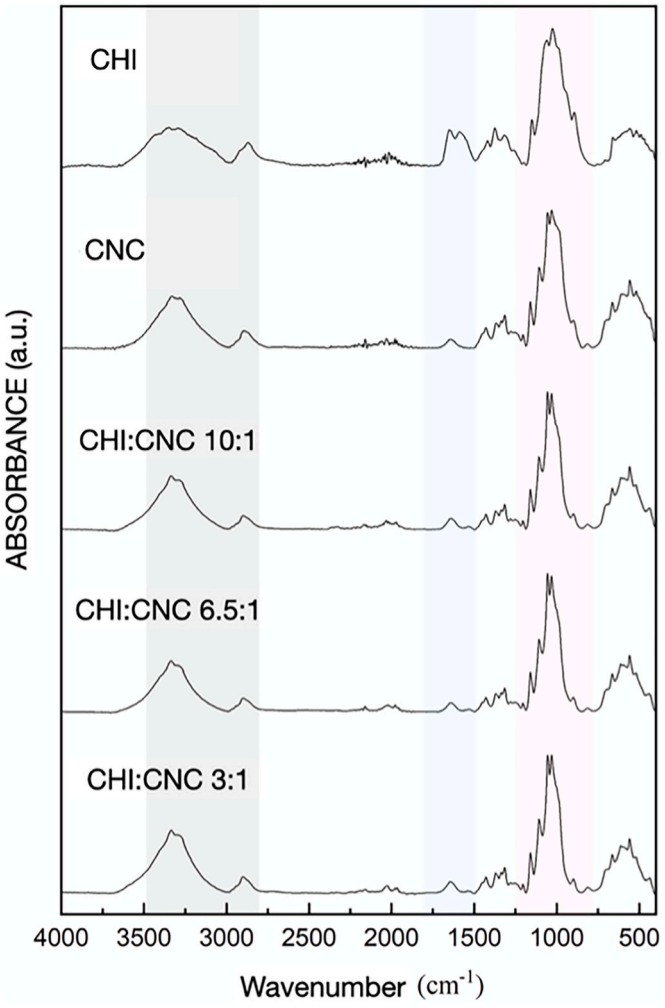

Fig. 4. Fourier Transform Infrared Spectroscopy spectra of chitosan (CH), nanocrystalline cellulose (CNC), and CH:CNC nanocomplexes at different molar ratios.

The chitosan spectrum exhibited a broad band between 3050 and 3600 cm^{-1}, attributed to N—H and O—H stretching vibrations, a band at 2867 cm^{-1} due to axial C—H deformation, a peak at 1648 cm^{-1} corresponding to the bending vibration of the amide II band, a peak at 1589 cm^{-1} related to N—H bending vibrations, a peak at 1060 cm^{-1} referring to C—N stretching vibrations, and peaks between 890 cm^{-1} and 1149 cm^{-1} due to ether linkages.

Regarding CNC, it showed a band between 3580 and 3100 cm^{-1}, also associated with vibrations of hydroxyl (–OH) groups. The bands at 2892 cm^{-1} and between 1500 and 1250 cm^{-1} correspond to stretching and bending vibrations of CH and CH_2 groups, respectively. These bands are characteristic of cellulosic materials and are consistent with those reported by Abo-Elseoud et al. [32] and Wang and Roman [24]. The peak at 1641 cm^{-1} corresponds to adsorbed water, while peaks at 1429 cm^{-1}, 1160 cm^{-1}, and 1054 cm^{-1} refer to C—O stretching vibrations, glycosidic bonds, and primary and secondary hydroxyl groups (C—O), respectively [32].

The nanocomplexes presented spectra very similar to CNC, with no characteristic peaks of chitosan, indicating the predominant presence of CNC in the formed structures. However, subtle changes in intensity compared to chitosan and CNC were observed, such as at the peak at 896 cm^{-1}, related to out-of-plane OH bending vibrations, and the shift of the peak at 1648 cm^{-1}, attributed to the bending vibration of chitosan's amide II band, which varied between 4 and 6 cm^{-1} among the nanocomplexes when CNC was added. This suggests that, even though CNC was present in greater quantity, interactions between CNC and chitosan were established, mainly hydrogen bonding. This is supported by the disappearance of the band at 3430 cm^{-1}, corresponding to the N—H stretching vibration associated with chitosan, and the shift and increase in intensity of the peaks at 3334 cm^{-1} in the nanocomplexes compared to 3326 cm^{-1} for CNC alone [32,33].

3.5. Thermogravimetric analysis

Thermogravimetric analysis (TGA) was conducted on samples of chitosan, CNC, and the formed nanocomplexes (NP 3:1, NP 6.5:1, and NP 10:1). The TGA and the derivative thermogravimetric (DTG) curves can be seen in Fig. 5.

Table 4 shows the temperatures corresponding to each thermal event of the studied systems, along with the associated percentage of mass loss (for details, see Supplementary Material; Figs. SM4 and SM5). Chitosan degraded in three stages, the first being an endothermic event. The percentage mass loss in this region was 9.33 %, attributed to the evaporation of adsorbed water within the polymer [34]. The second event, this time exothermic and observed between 254 and 345 °C, is highlighted as the most significant by [34], as it is associated with chitosan depolymerisation, including deacetylation and cleavage of glycosidic bonds through dehydration and deamination, starting with the breakage of the C–O–C bond [34,35]. The third event, occurring between 360 and 420 °C, corresponds to the degradation of cross-linked chitosan residues and accounts for a 23.7 % mass loss.

The DTG curves also reveal a maximum thermal decomposition rate of 0.0058 mg/°C. At the end of the process, a residual mass remains, indicating the presence of non-volatile components in chitosan [6]. The same behaviour was observed for CNC and the formed nanocomplexes.

For the CNC, the first event occurred between 32 and 108 °C, corresponding to a mass loss of 3.65 %, attributed to the evaporation of adsorbed water and water bound within the cellulosic structure and/or adsorbed low molecular weight compounds [36]. The peak between 273 and 318 °C is ascribed to various degradation processes of the CNC, such as depolymerisation, dehydration, and decomposition of the glycosidic units [37], showing a high degradation rate of 0.0177 mg/°C and a corresponding mass loss of 48.7 %. The third degradation event,

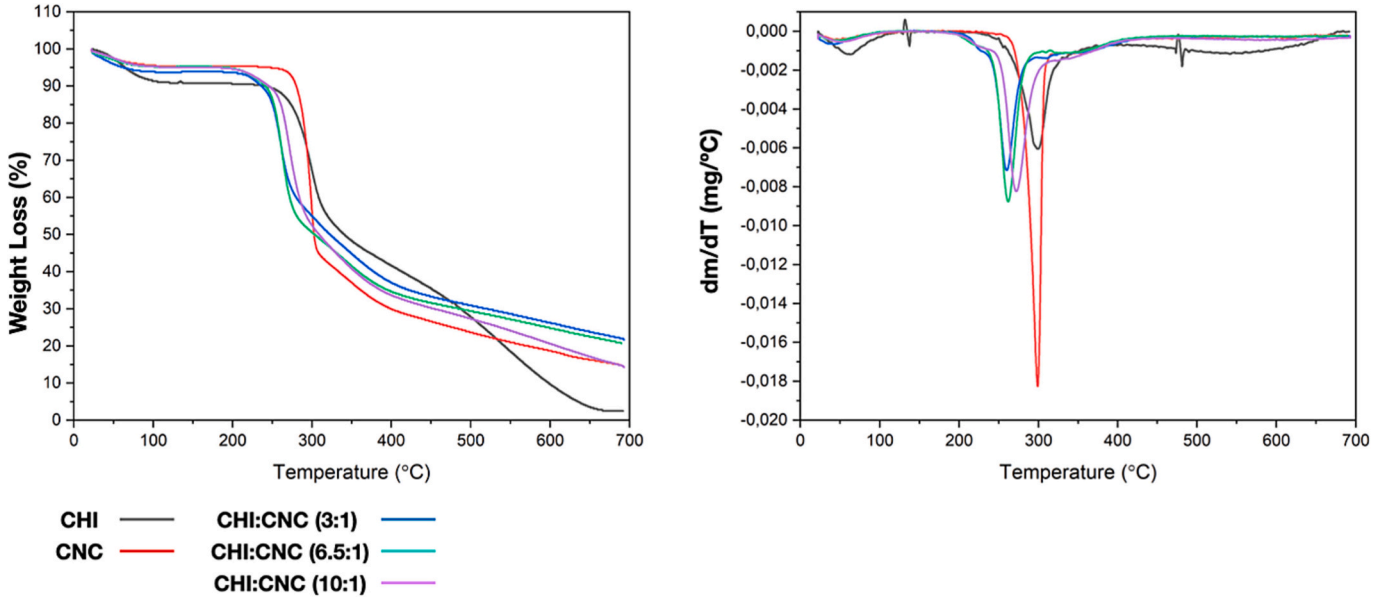

Fig. 5. Thermogravimetric analysis and derivative thermogravimetric thermograms of Chitosin (CH), nanocrystalline cellulose (CNC), and chitosan: nanocrystalline cellulose nanocomplexes at different molar ratios.

Table 4
Thermal decomposition temperatures and mass loss (%) of chitosan (CH), nanocrystalline cellulose (CNC), and nanocomplexes.

SYSTEM		T_I*	$T_{inflection\ point}$	T_F**	Weight loss (%)	Total weight loss (%)
CHI	1	25	63	116	9.33	74.75
	2	254	304.6	345	41.68	
	3	441.4	561	686.8	23.74	
CNC	1	32	45.7	108.2	3.65	69.48
	2	273.9	305.09	318.3	48.68	
	3	318.3	364.7	423.78	17.15	
CHI:CNC 3:1	1	25	41.7	104.9	5.63	64.97
	2	230.3	262.6	290.8	33.34	
	3	332.8	367	433.5	26	
CHI:CNC 6.5:1	1	30	51.9	105	3.94	65.5
	2	235	269	299	40.45	
	3	322.7	355.5	436	21.11	
CHI:CNC 10:1	1	25	50.6	106.6	4.32	65.39
	2	248.5	272.2	298.3	39.63	
	3	320	352.7	415	21.44	

occurring between 318 and 423.8 °C, is primarily attributed to the breakdown of charged fragments with the formation of low molecular weight gaseous products [37].

The thermograms of the nanocomplexes exhibited degradation peaks in similar regions, comprising three thermal events. The first, with a minimum temperature between 41 °C and 51 °C and mass loss between 4 % and 6 %, is attributed to the loss of physically adsorbed water and water strongly bound through hydrogen bonds in both the pure polymers and the nanocomplexes [23,31]. The second event, with minimum temperatures of 262.6 °C, 269 °C, and 272 °C for CHI:CNC 3:1, CHI:CNC 6.5:1, and NP 10:1 respectively, corresponds to mass loss from degradation of the polymer chains of chitosan, CNC, and the CHI-CNC structures formed, involving decomposition of the pyranose structure due to dehydration, resulting in ring opening [38]. A reduction in the thermal stability of the nanocomplexes was also observed with increasing content of sulfonate groups (-OSO3-) compared to the pure polymers. This can be explained by the greater sensitivity of these groups to heating, which facilitates the thermal degradation of the nanocomplexes [39]. Moreover, as the molar amount of CNC in the system decreases, fewer electrostatic interactions and hydrogen bonds are established with chitosan, requiring lower temperatures and consequently less energy to degrade the formed structures [6,38].

The third event, with minimum temperatures at 367 °C, 355.5 °C, and 352.7 °C for NP 3:1, NP 6.5:1, and NP 10:1 respectively, corresponds to mass losses of 26 %, 21.11 %, and 21.44 %, respectively. This is related to the carbonisation of polymeric residues and volatilisation reactions of low molecular weight compounds [38], being most intense in the CHI:CNC 3:1 nanocomplex, which exhibits 26 % mass loss compared to 21.11 % and 21.44 % in CHI:CNC 6.5:1 and CHI:CNC 10:1 respectively. This phenomenon is attributed to the higher sensitivity to heating of the cellulose nanocrystal, as previously mentioned.

Although the thermal stability of the nanocomplexes is lower compared to chitosan and CNC alone, based on the total mass loss of chitosan, CNC, and the nanocomplexes, it can be concluded that the formation of these new supramolecular structures contributed to an improvement in the thermal resistance of the nanocomplexes, as evidenced by the greater residual mass detected at the end of thermodegradation compared to the pure polymers.

3.6. Macroscopic and microscopic stability

The visual appearance and Tyndall scattering effects of systems (CHI:CNC = 3:1; 6.5:1; or 10:1) stored at 25 °C and 7 °C were recorded over a 30-day period to observe changes in their macroscopic stability. The results are presented in Figs. 6 and 7.

All the developed nanocomplexes were observed as colloidal dispersions, i.e., systems without aggregate formation or sedimented particles. This observation is supported by the concentrations of polymers used (0.5 $mg{\cdot}mL^{-1}$ for chitosan and 1 $mg{\cdot}mL^{-1}$ for CNC) and the proportions employed, as opalescent colloidal systems with fine particles in suspension are predominantly formed by diluted polyelectrolyte dispersions in non-stoichiometric ratios, characterising polyelectrolyte complexes [40]. The degree of opalescence of the dispersions increased as the CHI:CNC ratio decreased. This can be explained by the molar ratio of functional groups (NH_3^+ in CHI and OSO_3^- in CNC) approaching unity, which may have intensified inter- and intramolecular interactions and promoted greater formation of nanocomplexes [24].

Figs. 6 and 7 illustrate this effect in the produced nanocomplexes. At 25 °C, greater instability was observed in the 10:1 ratio, where, by day 30, evident flocculation occurred, impeding continuous passage of the

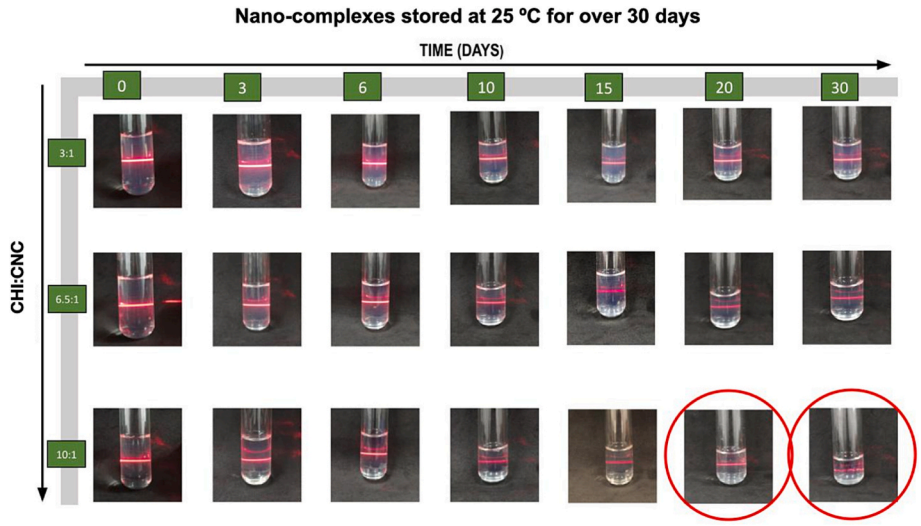

Fig. 6. Visual aspect and Tyndall effect of systems containing chitosan: nanocrystalline cellulose nanocomplexes at different molar ratio stored during 30 days (25 °C).

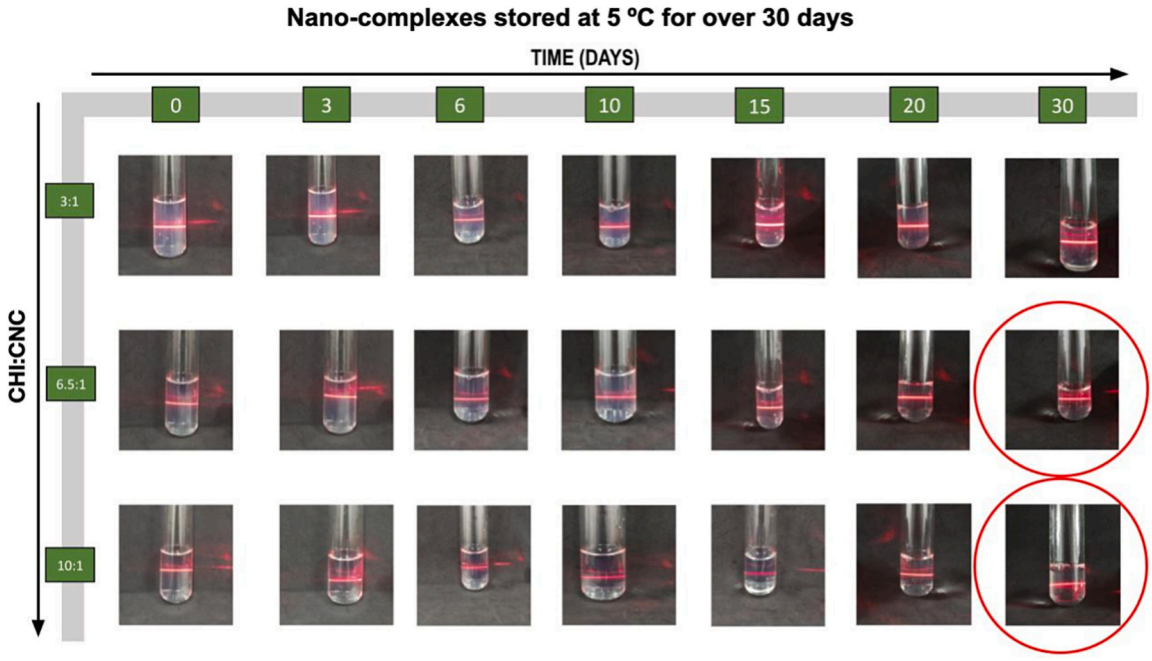

Fig. 7. Visual aspect and Tyndall effect of systems containing chitosan: nanocrystalline cellulose nanocomplexes at different molar ratio stored during 30 days (7 °C).

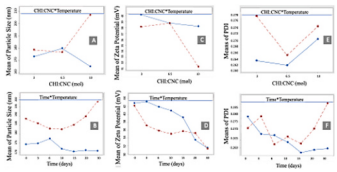

Fig. 8. Interaction effects plots from the interaction between different independent variables for dependent variables: molar ratio and temperature for Particle size (A); molar ratio and time for Particle size (B); molar ratio and temperature for Zeta-potential (C); and molar ratio and time for Zeta-potential (D); molar ratio and temperature for polydispersity index (PDI) (E); and molar ratio and time for PDI (F).

laser beam. A similar observation was made for the 6.5:1 and 10:1 dispersions stored at 7 °C, with the higher ratio again promoting greater laser refraction. According to [24], when a chitosan dispersion is titrated with CNC, bridging flocculation can occur due to the excess molar amount of chitosan present in the reaction medium, which, at low pH (pH = 3 in this study), adopts an extended configuration with most amino groups protonated. Consequently, when CNC is added dropwise to the chitosan dispersion, more than one CNC chain may adsorb onto the chitosan molecule surface, causing destabilisation.

To examine the behaviour of the studied variables, interaction plots were generated for each. The factorial experiment analysis revealed significant ($p < 0.05$) interaction effects between time and temperature, as well as CHI:CNC ratio and temperature, for all variables studied. Fig. 8 presents interaction plots of adjusted mean values for size, zeta potential, and polydispersity index (PDI) as a function of time at 7 °C and 25 °C (Fig. 8B, D, and F) and as a function of CHI:CNC ratio at both

temperatures (Fig. 8A, C, and E), allowing evaluation of apparent interaction effects and the behaviour of Particle size, zeta potential, and PDI with respect to these variables.

Evaluating the nanocomplex size, it is evident that among the ratios studied, CHI:CNC = 10:1 was the most unstable. Nanocomplexes produced at this ratio exhibited initially larger sizes compared to those at 3:1 and 6.5:1, with sizes increasing over storage time, as shown in Figs. 6 and 7. One of the main factors governing the formation and stability of polyelectrolyte complexes (PECs) formed by weak polyelectrolytes is pH. The formulated systems were prepared at pH 5 and redispersed in Milli-Q water. In the absence of salts, PEC formation is rapid and can lead to a thermodynamically less stable system due to low osmotic pressure of the diluent [41]. Thus, water molecules can penetrate the nanocomplexes via osmosis and cause swelling, potentially leading to size increases during storage [42]. Furthermore, the inherent Brownian motion of particles in dispersion may have intensified at certain points during storage due to minor temperature fluctuations, increasing collision frequency among nanocomplexes and facilitating particle adhesion, thereby forming small flocs and/or aggregates by the end of storage [42].

The PDI and zeta potential results complement the Particle size data, showing that after 15 days of storage at 25 °C, the CHI:CNC = 10:1 system becomes more heterogeneous, with PDI values exceeding 0.3 and a lower zeta potential, especially from day 20 onwards, reaching 26 mV. Reductions in zeta potential and increases in system heterogeneity during storage may be attributed to pH changes resulting from shifts in the chemical equilibrium of the dispersions due to salt absence [43]. Considering the data presented, the formulations can be ranked by stability as follows: 3:1 > 6.5:1 > 10:1, with the 3:1 ratio showing no sedimentation after 30 days of storage.

4. Conclusion

The chitosan and nanocrystalline cellulose nanocomplexes developed in this study demonstrated promising physicochemical and thermal properties, underscoring their potential for food-related applications such as encapsulation, stabilization, and controlled release systems. For the different CHI:CNC ratios (3; 6.5; and 10), NaCL concentration (0–37.5 mM), and pH values (2.6–5), the polyelectrolytes presented size of 151–195 nm, polydispersity indices (PDI) of 0.26–0.30, and potential zeta of 44–52 mV. Process yield was highest for the CHI:CNC 3:1 system (4.7–7.1 %), compared with 2.6–6.7 % for the other ratios. Therefore, optimization indicated that 3:1 CHI:CNC at pH 5.0 and without NaCl addition was the smallest (~165 nm) most highly charged (~46 mV) nanoparticle and achieved yield of around 7 %. Stability evaluations, including the 6.5 and 10 systems for comparison, were carried out through visual inspection and Tyndall scattering. CHI:CNC 3:1 nanocomplex was the most stable, showing no visible aggregation or sedimentation over 30 days at both 7 °C and 25 °C, while maintaining 170–180 nm size, 0.26–0.28 PDI and 37–40 mV properties. In contrast, the 6.5 and 10 polyelectrolites showed destabilisation, particularly at 7 °C. Brownian motion and minor temperature fluctuations likely promoted particle collisions, leading aggregation over time. This long-term colloidal stability is a key indicator of system robustness for food formulation, particularly in aqueous matrices and under refrigerated or ambient conditions. Thermal results indicated three main degradation events for all formulations, ranging from 230 °C to 300 °C for main degradation and 320 °C to 436 °C for secondary degradation. These results confirm the suitability of nanocomplexes up to 280 °C, highlighting their applicability to food operation involving moderate to high heating, such as drying, baking, pasteurisation or sterilization processes. FTIR analysis further confirmed CNC characteristic bands (3580–3100 cm^{-1}, 2892 cm^{-1}, and 1250 cm^{-1}) and new hydrogen interactions, which may contribute to improved barrier and retention properties in delivery systems. In summary, this work demonstrated successfully the formation of CHI:CNC nanocomplexes with tunable physicochemical and thermal properties determined concomitantly by polymer ratio, NaCL concentration, and pH. The 3:1 CHI:CNC formulation at pH 5.0, without NaCl, was identified as the most stable formulation, making it a promising candidate for food industry applications requiring biocompatible, thermally stable, and colloidally delivery systems. A distinct contribution of this work is the comprehensive characterisation of CHI:CNC nanocomplexes in their isolated form, independent of any specific active compound, while simultaneously optimization key parameters (ph, NaCl, CHI:CNC ratio) as functions of size, zeta potential, and yield. Unlike most previous studies, which have primarily focused on encapsulation or delivery of bioactive compounds, this approach provide fundamental insights into the intrinsic stability and behaviour of the base nanocomplexe system. Such knowledge is essential for guiding the design and optimization of a broad range of functional delivery systems in both food and pharmaceutical applications.

CRediT authorship contribution statement

Rafaela Venâncio Flores: Writing – original draft, Investigation, Data curation. **Meirielly Jesus:** Writing – review & editing, Writing – original draft. **Joana Santos:** Writing – review & editing, Writing – original draft. **Fernando Mata:** Writing – review & editing, Writing – original draft. **Lucas de Souza Soares:** Writing – original draft, Investigation, Data curation. **Eduardo Basilio de Oliveira:** Formal analysis, Data curation, Conceptualization. **Sukarno Olavo Ferreira:** Formal analysis, Data curation, Conceptualization. **Taíla Veloso de Oliveira:** Writing – review & editing, Project administration, Conceptualization. **Nilda de Fátima Ferreira Soares:** Writing – review & editing, Project administration, Conceptualization.

Funding

The authors wish to acknowledge the financial support provided by Coordination of Higher Education Personnel Improvement, Brazil (CAPES—n° 001).

Declaration of competing interest

The authors declare the following financial interests/personal relationships which may be considered as potential competing interests: Nilda Soares reports financial support was provided by Coordination of Higher Education Personnel Improvement. If there are other authors, they declare that they have no known competing financial interests or personal relationships that could have appeared to influence the work reported in this paper.

Acknowledgements

To the Foundation for Science and Technology (FCT, Portugal) for financial support to the Center for Research and Development in Agri-food Systems and Sustainability (CISAS) [UIDB/05937/2020 (doi.org/10.54499/UIDB/05937/2020) and UIDP/05937/2020 (doi.org/10.54499/UIDP/05937/2020)].

Appendix A. Supplementary data

Supplementary data to this article can be found online at https://doi.org/10.1016/j.ijbiomac.2025.147212.

Data availability

Data will be made available upon reasonable request.

References

[1] V.S. Meka, M.K.G. Sing, M.R. Pichika, S.R. Nali, V.R.M. Kolapalli, P. Kesharwani, A comprehensive review on polyelectrolyte complexes, Drug Discov. Today 22 (11) (2017) 1697–1706, https://doi.org/10.1016/j.drudis.2017.06.008.

[2] H. Wang, C. Qian, M. Roman, Effects of pH and salt concentration on the formation and properties of chitosan–cellulose nanocrystal polyelectrolyte–macroion complexes, Biomacromolecules 12 (10) (2011) 3708–3714, https://doi.org/10.1021/bm2009685.

[3] D. Wu, L. Zhu, Y. Li, X. Zhang, S. Xu, G. Yang, T. Delair, Chitosan-based colloidal polyelectrolyte complexes for drug delivery: a review, Carbohydr. Polym. 238 (2020) 116126, https://doi.org/10.1016/j.carbpol.2020.116126.

[4] Q. Xu, Y. Ji, Q. Sun, Y. Fu, Y. Xu, L. Jin, Fabrication of cellulose nanocrystal/chitosan hydrogel for controlled drug release, Nanomaterials 9 (2) (2019) 253, https://doi.org/10.3390/nano9020253.

[5] R.M. Bulatao, J.P.A. Samin, J.R. Salazar, J.J. Monserate, Encapsulation of anthocyanins from black rice (Oryza sativa L.) bran extract using chitosan-alginate nanoparticles, 2017, https://doi.org/10.5539/jfr.v6n3p40.

[6] D.C.M. Ferreira, S.O. Ferreira, E.S. de Alvarenga, N. de F.F. Soares, J.S. dos Reis Coimbra, E.B. de Oliveira, Polyelectrolyte complexes (PECs) obtained from chitosan and carboxymethylcellulose: a physicochemical and microstructural study, Carbohydr. Polym. Technol. Appl. 3 (2022) 100197, https://doi.org/10.1016/j.carpta.2022.100197.

[7] W. Wang, J. Jung, Y. Zhao, Chitosan-cellulose nanocrystal microencapsulation to improve encapsulation efficiency and stability of entrapped fruit anthocyanins, Carbohydr. Polym. 157 (2017) 1246–1253, https://doi.org/10.1016/j.carbpol.2016.11.005.

[8] M.G. Paulraj, S. Ignacimuthu, M.R. Gandhi, A. Shajahan, P. Ganesan, S. M. Packiam, N.A. Al-Dhabi, Comparative studies of tripolyphosphate and glutaraldehyde cross-linked chitosan-botanical pesticide nanoparticles and their agricultural applications, Int. J. Biol. Macromol. 104 (2017) 1813–1819, https://doi.org/10.1016/j.ijbiomac.2017.06.043.

[9] S.P. Akhlaghi, D. Tiong, R.M. Berry, K.C. Tam, Comparative release studies of two cationic model drugs from different cellulose nanocrystal derivatives, Eur. J. Pharm. Biopharm. 88 (1) (2014) 207–215, https://doi.org/10.1016/j.ejpb.2014.04.012.

[10] H. Xie, H. Du, X. Yang, C. Si, Recent strategies in preparation of cellulose nanocrystals and cellulose nanofibrils derived from raw cellulose materials, Int. J. Polym. Sci. 2018 (1) (2018) 7923068, https://doi.org/10.1155/2018/7923068.

[11] H. Jonassen, A.-L. Kjøniksen, M. Hiorth, Effects of ionic strength on the size and compactness of chitosan nanoparticles, Colloid Polym. Sci. 290 (2012) 919–929, https://doi.org/10.1007/s00396-012-2604-3.

[12] I.J. Joye, G. Davidov-Pardo, D.J. McClements, Nanotechnology for increased micronutrient bioavailability, Trends Food Sci. Technol. 40 (2) (2014) 168–182, https://doi.org/10.1016/j.tifs.2014.08.006.

[13] G.T.F. da S. Furtado, T.B. Fideles, R. de C.A.L. Cruz, J.W. de L. Souza, M. A. Rodriguez Barbero, M.V.L. Fook, Chitosan/NaF particles prepared via ionotropic gelation: evaluation of particles size and morphology, Mater. Res. 21 (2018) e20180101, https://doi.org/10.1590/1980-5373-MR-2018-0101.

[14] S.J.S. Chelladurai, K. Murugan, A.P. Ray, M. Upadhyaya, V. Narasimharaj, S. Gnanasekaran, Optimization of process parameters using response surface methodology: a review, Mater. Today Proc. 37 (2021) 1301–1304, https://doi.org/10.1016/j.matpr.2020.06.466.

[15] S. Sreekumar, F.M. Goycoolea, B.M. Moerschbacher, G.R. Rivera-Rodriguez, Parameters influencing the size of chitosan-TPP nano-and microparticles, Sci. Rep. 8 (1) (2018) 4695, https://doi.org/10.1038/s41598-018-23064-4.

[16] L. de Souza Soares, G.L. Milião, B. Tonole, G.B. de Souza, N. de F.F. Soares, A.V. N. de Carvalho Teixeira, J.S. dos Reis Coimbra, E.B. de Oliveira, Chitosan dispersed in aqueous solutions of acetic, glycolic, propionic or lactic acid as a thickener/stabilizer agent of O/W emulsions produced by ultrasonic homogenization, Ultrason. Sonochem. 59 (2019) 104754, https://doi.org/10.1016/j.ultsonch.2019.104754.

[17] M.L. Amorim, G.M.D. Ferreira, L. de S. Soares, W.A. dos S. Soares, A.M. Ramos, J.S. dos R. Coimbra, L.H.M. da Silva, E.B. de Oliveira, Physicochemical aspects of chitosan dispersibility in acidic aqueous media: effects of the food acid counter-anion, Food Biophys. 11 (2016) 388–399, https://doi.org/10.1007/s11483-016-9453-4.

[18] M.R. Kasaai, Calculation of Mark–Houwink–Sakurada (MHS) equation viscometric constants for chitosan in any solvent–temperature system using experimental reported viscometric constants data, Carbohydr. Polym. 68 (3) (2007) 477–488, https://doi.org/10.1016/j.carbpol.2006.11.006.

[19] J. Brugnerotto, J. Lizardi, F.M. Goycoolea, W. Argüelles-Monal, J. Desbrieres, M. Rinaudo, An infrared investigation in relation with chitin and chitosan characterization, Polymer 42 (8) (2001) 3569–3580, https://doi.org/10.1016/S0032-3861(00)00713-8.

[20] S. Beck, M. Méthot, J. Bouchard, General procedure for determining cellulose nanocrystal sulfate half-ester content by conductometric titration, Cellulose 22 (2015) 101–116, https://doi.org/10.1007/s10570-014-0513-y.

[21] L. Segal, J.J. Creely, A.E. Martin Jr., C.M. Conrad, An empirical method for estimating the degree of crystallinity of native cellulose using the X-ray diffractometer, Text. Res. J. 29 (10) (1959) 786–794, https://doi.org/10.1177/004051755902901.

[22] G.A. Morris, J. Castile, A. Smith, G.G. Adams, S.E. Harding, The effect of prolonged storage at different temperatures on the particle size distribution of tripolyphosphate (TPP)–chitosan nanoparticles, Carbohydr. Polym. 84 (4) (2011) 1430–1434, https://doi.org/10.1016/j.carbpol.2011.01.044.

[23] W.K. Delan, M. Zakaria, B. Elsaadany, A.N. ElMeshad, W. Mamdouh, A.R. Fares, Formulation of simvastatin chitosan nanoparticles for controlled delivery in bone regeneration: optimization using Box-Behnken design, stability and in vivo study, Int. J. Pharm. 577 (2020) 119038, https://doi.org/10.1016/j.ijpharm.2020.119038.

[24] H. Wang, M. Roman, Formation and properties of chitosan−cellulose nanocrystal polyelectrolyte−macroion complexes for drug delivery applications, Biomacromolecules 12 (5) (2011) 1585–1593, https://doi.org/10.1021/bm101584c.

[25] R. Prathapan, R. Thapa, G. Garnier, R.F. Tabor, Modulating the zeta potential of cellulose nanocrystals using salts and surfactants, Colloids Surf. A Physicochem. Eng. Asp. 509 (2016) 11–18, https://doi.org/10.1016/j.colsurfa.2016.08.075.

[26] P. Mukhopadhyay, K. Sarkar, M. Chakraborty, S. Bhattacharya, R. Mishra, P. P. Kundu, Oral insulin delivery by self-assembled chitosan nanoparticles: in vitro and in vivo studies in diabetic animal model, Mater. Sci. Eng. C 33 (1) (2013) 376–382, https://doi.org/10.1016/j.msec.2012.09.001.

[27] M. Anand, P. Sathyapriya, M. Maruthupandy, A.H. Beevi, Synthesis of chitosan nanoparticles by TPP and their potential mosquito larvicidal application, Front. Lab. Med. 2 (2) (2018) 72–78, https://doi.org/10.1016/j.flm.2018.07.003.

[28] M.W. Wildan, F.I. Lubis, Fabrication and characterization of chitosan/cellulose nanocrystal/glycerol bio-composite films, Polymers 13 (7) (2021) 1096, https://doi.org/10.3390/polym13071096.

[29] E. Zhang, R. Xing, S. Liu, Y. Qin, K. Li, P. Li, Advances in chitosan-based nanoparticles for oncotherapy, Carbohydr. Polym. 222 (2019) 115004, https://doi.org/10.1016/j.carbpol.2019.115004.

[30] Y. Jampafuang, A. Tongta, Y. Waiprib, Impact of crystalline structural differences between α-and β-chitosan on their nanoparticle formation via ionic gelation and superoxide radical scavenging activities, Polymers 11 (12) (2019) 2010, https://doi.org/10.3390/polym11122010.

[31] H. Celebi, A. Kurt, Effects of processing on the properties of chitosan/cellulose nanocrystal films, Carbohydr. Polym. 133 (2015) 284–293, https://doi.org/10.1016/j.carbpol.2015.07.007.

[32] W.S. Abo-Elseoud, M.L. Hassan, M.W. Sabaa, M. Basha, E.A. Hassan, S.M. Fadel, Chitosan nanoparticles/cellulose nanocrystals nanocomposites as a carrier system for the controlled release of repaglinide, Int. J. Biol. Macromol. 111 (2018) 604–613, https://doi.org/10.1016/j.ijbiomac.2018.01.044.

[33] A.L. de Pinho Neves, C.C. Milioli, L. Müller, H.G. Riella, N.C. Kuhnen, H.K. Stulzer, Factorial design as tool in chitosan nanoparticles development by ionic gelation technique, Colloids Surf. A Physicochem. Eng. Asp. 445 (2014) 34–39, https://doi.org/10.1016/j.colsurfa.2013.12.058.

[34] F.A. López, A.L.R. Mercê, F.J. Alguacil, A. López-Delgado, A kinetic study on the thermal behaviour of chitosan, J. Therm. Anal. Calorim. 91 (2) (2008) 633–639, https://doi.org/10.1007/s10973-007-8321-3.

[35] K. Xu, C. Liu, K. Kang, Z. Zheng, S. Wang, Z. Tang, W. Yang, Isolation of nanocrystalline cellulose from rice straw and preparation of its biocomposites with chitosan: physicochemical characterization and evaluation of interfacial compatibility, Compos. Sci. Technol. 154 (2018) 8–17, https://doi.org/10.1016/j.compscitech.2017.10.022.

[36] M.A. Henrique, W.P. Flauzino Neto, H.A. Silvério, D.F. Martins, L.V.A. Gurgel, H. da S. Barud, L.C. de Morais, D. Pasquini, Kinetic study of the thermal decomposition of cellulose nanocrystals with different polymorphs, cellulose I and II, extracted from different sources and using different types of acids, Ind. Crop. Prod. 76 (2015) 128–140, https://doi.org/10.1016/j.indcrop.2015.06.048.

[37] M. Roman, W.T. Winter, Effect of sulfate groups from sulfuric acid hydrolysis on the thermal degradation behavior of bacterial cellulose, Biomacromolecules 5 (5) (2004) 1671–1677, https://doi.org/10.1021/bm034519.

[38] S. Bonardd, E. Robles, I. Barandiaran, C. Saldías, Á. Leiva, G. Kortaberria, Biocomposites with increased dielectric constant based on chitosan and nitrile-modified cellulose nanocrystals, Carbohydr. Polym. 199 (2018) 20–30, https://doi.org/10.1016/j.carbpol.2018.06.088.

[39] D.T. Zvezdova, Identification of kinetics models for non-isothermal decomposition of solids from thermogravimetric analysis: kinetic analysis of chitin of shrimp shell from Black Sea, J. Therm. Anal. Calorim. 149 (14) (2024) 7355–7365, https://doi.org/10.1007/s10973-024-13338-7.

[40] V.S. Rathee, H. Sidky, B.J. Sikora, J.K. Whitmer, Role of associative charging in the entropy–energy balance of polyelectrolyte complexes, J. Am. Chem. Soc. 140 (45) (2018) 15319–15328, https://doi.org/10.1021/jacs.8b08649.

[41] H. Wang, C. Qian, M. Roman, Effects of pH and salt concentration on the formation and properties of chitosan–cellulose nanocrystal polyelectrolyte–macroion complexes, Biomacromolecules 12 (10) (2011) 3708–3714, https://doi.org/10.1021/bm200968.

[42] M.-L. Tsai, R.-H. Chen, S.-W. Bai, W.-Y. Chen, The storage stability of chitosan/tripolyphosphate nanoparticles in a phosphate buffer, Carbohydr. Polym. 84 (2) (2011) 756–761, https://doi.org/10.1016/j.carbpol.2010.04.040.

[43] H. Jonassen, A.-L. Kjøniksen, M. Hiorth, Effects of ionic strength on the size and compactness of chitosan nanoparticles, Colloid Polym. Sci. 290 (2012) 919–929, https://doi.org/10.1007/s00396-012-2604-3.

[44] I.D. Souza, V. Saez, C.R. Mansur, Lipid nanoparticles containing coenzyme Q10 for topical applications: An overview of their characterization, Col. Surf. B Biointerf. 230 (2023) 113491, https://doi.org/10.1016/j.colsurfb.2023.113491.